PAPER

Check for updates

Cascaded elasto-inertial separation of malignant tumor cells from untreated malignant pleural and peritoneal effusions†

Chen Ni,[a] Dan Wu,[b] Yao Chen,[a] Silin Wang[a] and Nan Xiang (iD) *[a]

Separation of malignant tumor cells (MTCs) from large background cells in untreated malignant pleural and peritoneal effusions (MPPEs) is critical for improving the sensitivity and efficiency of cytological diagnosis. Herein, we proposed a cascaded elasto-inertial cell separation (CEICS) device integrating an interfacial elasto-inertial microfluidic channel with a symmetric contraction expansion array (CEA) channel for pretreatment-free, high-recovery-ratio, and high-purity separation of MTCs from clinical MPPEs. First, the effects of flow-rate ratio, cell concentration, and cell size on separation performances in two single-stage channels were investigated. Then, the performances of the integrated CEICS device were characterized using blood cells spiked with three different tumor cells (MCF-7, MDA-MB-231, and A549 cells) at a high total throughput of 240 μL min^{-1}. An average recovery ratio of ~95% and an average purity of ~61% for the three tumor cells were achieved. Finally, we successfully applied the CEICS device for the pretreatment-free separation of MTCs from clinical MPPEs of different cancers. Our CEICS device may provide a preparation tool for improving the sensitivity and efficiency of cytological examination.

1. Introduction

Pleural and peritoneal effusions refer to the abnormal accumulation of exudate in pleural and peritoneal cavities and are common medical problems caused by various diseases.[1–3] Malignant pleural and peritoneal effusions (MPPEs) caused by metastatic malignancy significantly deteriorate the patient functional capacity and life quality.[4–6] Typically, the malignancy of pleural and peritoneal effusions is diagnosed through manually counting malignant tumor cells (MTCs) in effusions by an experienced clinical pathologist.[7] However, the presence of a large number of background blood cells in pleural and peritoneal effusions significantly compromises the sensitivity of cytological diagnosis.[8,9] Therefore, the separation of MTCs from a large number of background cells in MPPEs is beneficial to improve the sensitivity and efficiency of cytological diagnosis, which is of great importance for the diagnosis and prognosis assessment of cancer patients.

The advent of microfluidics provides new insights into the separation of target cells from complex background in a low-cost, user-friendly, and high-precision manner.[10–13] In particular, passive microfluidic technologies[14–17] utilize the intrinsic hydrodynamic forces induced by the designed microchannel structures to manipulate cells and thus own the advantages of simplicity and autonomy. Passive microfluidic technologies have been widely used for the separation of target cells in high cell concentration samples (such as circulating tumor cells[18–20] in peripheral blood and MTCs[21–23] in MPPEs) as it provides a high processing throughput up to 1–5 mL min^{-1}.[24–26] Currently, passive microfluidic cell separation technologies mainly include inertial microfluidics,[27] viscoelastic microfluidics,[28,29] deterministic lateral displacement,[30,31] *etc.* The most attention has been paid to inertial microfluidics because the cell separation can be achieved *via* inertial lift force[32] and Dean drag force[33] over a wide range of Reynolds numbers (1–100). However, the previous inertial microfluidics[34–36] for MTC separation found it difficult to handle samples with high cell concentrations. To ensure separation performance, lysis pretreatment of red blood cells (RBCs) was required (see Table S1†), which complicated the operation. The RBC lysis buffer may destroy MTCs, reducing the detection sensitivity. In addition, due to the limited separation accuracy of inertial microfluidics, the purity of the separated MTCs remains low.

Through adding an additional elastic force[37] induced by the viscoelastic fluids, viscoelastic microfluidics can achieve a higher cell separation precision and flexibility than inertial

[a] School of Mechanical Engineering, and Jiangsu Key Laboratory for Design and Manufacture of Micro-Nano Biomedical Instruments, Southeast University, Nanjing, 211189, China. E-mail: nan.xiang@seu.edu.cn

[b] Department of Oncology, Jiangyin People's Hospital, Jiangyin, 214400, China

† Electronic supplementary information (ESI) available. See DOI: https://doi.org/10.1039/d3lc00801k

microfluidics. Compared to single-phase viscoelastic microfluidics, interfacial viscoelastic microfluidics can further expand the lateral distance between cells of different sizes, thereby improving the separation performance. Li et al.[38] applied interfacial viscoelastic microfluidics for the separation of small bacterium, and successfully achieved the size-based separation of Staphylococcus epidermidis (S. epidermidis) and Lactobacillus rhamnosus (L. rhamnosus) and the shape-based separation of Escherichia coli (E. coli) and L. rhamnosus in a simple straight microchannel. Sun et al.[39] analyzed the effect of fluid media on particle separation in interfacial microfluidics. Compared with the sole use of Newtonian fluid or viscoelastic fluid, the co-flow system of Newtonian fluid and viscoelastic fluid could produce a stable elasto-inertial interface effect and improve the separation precision. After optimizing the cross-sectional dimension of the microchannel, they successfully realized the efficient separation of tumor cells in whole blood.[40] However, current interfacial elasto-inertial microfluidics[38-46] mainly used polyethylene oxide (PEO) solution, resulting in low processing throughput of $1-20~\mu L~min^{-1}$ (see Table S2†). To improve the sample processing throughput, we attempted to use hyaluronic acid (HA) solution instead of PEO solution.[47] Compared with other interfacial elasto-inertial microfluidics, we increased the sample flow rate by an order of magnitude while ensuring a high recovery rate of tumor cells and a high removal rate of blood cells. Although our interfacial elasto-inertial microfluidic[47] may handle samples with at higher cell concentrations, cell-to-cell interactions at high cell concentrations are still unavoidable, which may weaken the separation performance. Therefore, multi-stage separation of cells on a single chip may be a good strategy. In addition, due to the heterogeneity and complexity of clinical samples, achieving pretreatment-free, high-recovery-ratio, and high-purity separation of MTCs from clinical MPPEs remains to be a significant challenge.

In this paper, we developed a cascaded elasto-inertial cell separation (CEICS) device that integrated an interfacial elasto-inertial microfluidic channel with a symmetric contraction expansion array (CEA) channel to achieve pretreatment-free, high-recovery-ratio, and high-purity separation of MTCs from clinical MPPEs. The interfacial elasto-inertial microfluidic channel was employed to efficiently eliminate a significant quantity of blood cells, while the symmetric CEA channel was utilized for the subsequent removal of blood cells that had escaped from the first separation stage. After investigating the separation performances of single-stage channels, the integrated CEICS device was applied to the separation of tumor cells from blood cells. The experimental results demonstrated the excellent performances of our CEICS device for efficiently separating three tumor cells (MCF-7, MDA-MB-231, and A549 cells) with an average recovery ratio of ~95% and an average purity of ~61%. Compared with the single interfacial elasto-inertial microfluidic,[47] our CEICS device improved the purity of tumor cells by 2 to 4 times. Finally, we utilized our CEICS device to directly separate MTCs from untreated clinical MPPEs. All five clinical MPPE samples had detectable MTCs (45-270 cells per mL) with an average purity of ~24.62%. Compared with the previous inertial microfluidics for MTC separation, our CEICS device could handle samples with higher cell concentrations (see Table S1†). In addition, a high recovery ratio of MTCs could be achieved without the lysis of RBCs. We believed that our method could be useful for improving the sensitivity and efficiency of cytological diagnosis of MPPE samples.

2. Materials and methods

2.1 Working principle

Fig. 1A shows the workflow of our CEICS device for the pretreatment-free, high-recovery-ratio, and high-purity separation of MTCs from MPPE sample. The sample fluid and the sheath fluid containing hyaluronic acid were injected into the two side inlets and the middle inlet of the CEICS device at specific flow rates, respectively. The vast majority of RBCs and WBCs were removed by our CEICS device under the elasto-inertial effects, and then the enriched high-purity MTCs were identified and counted by immunofluorescence staining. To improve the separation precision, our CEICS device integrated an interfacial elasto-inertial microfluidic channel with a symmetric CEA channel to realize the two-stage separation of MTCs. During the interfacial elasto-inertial separation stage, cells were initially confined to both sides of the channel due to the pinch effect of the sheath fluid (I in Fig. 1B), and then gradually moved toward the fluid interface due to the inertial lift forces induced by the walls. Since the inertial lift forces acting on cells were proportional to their sizes, large MTCs moved rapidly toward the fluid interface and migrated across the fluid interface into the sheath fluid, while the small blood cells were blocked by the fluid interface and remained in the sample fluid. In addition, after entering the sheath fluid, the cells were additionally subjected to the elastic force pointing toward the channel center due to the viscoelasticity of sheath fluid, resulting in a gradual migration toward the channel center and a further increase in the lateral distance from the small cells (II in Fig. 1B). However, due to the heterogeneity of cell sizes and the collision between cells, a small part of blood cells might also pass through the fluid interface, thereby reducing the purity of the separated MTCs. Therefore, after the first-stage interfacial elasto-inertial separation, the cells entering the middle outlet were sorted again using the symmetric CEA channel. During the symmetric CEA separation stage, cells were subjected to the Dean drag force generated by the secondary flow in CEA structures, as well as the combined effects of inertial lift force and elastic force, and thus cells of different sizes were focused toward different equilibrium positions. Specifically, large MTCs would be focused at the channel center, while residual blood cells were distributed near both sides of the channel (III and IV in Fig. 1B), enabling the size-based separation of tumor cells and residual blood cells. Using this cascaded elasto-inertial separation device, the efficient removal
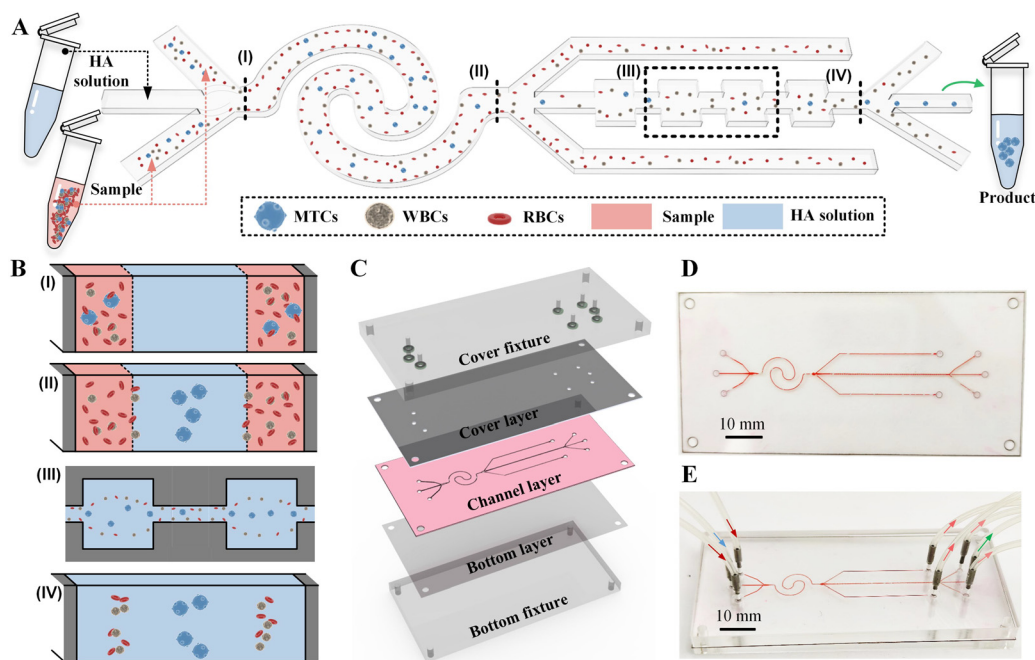
Fig. 1 (A) Schematic diagram illustrating the workflow of the proposed CEICS device for pretreatment-free, high-recovery-ratio, and high-purity separation of MTCs from blood cells. (B) Schematic diagram illustrating the cell migration at different positions of the CEICS device: (I) the channel inlet, (II) the outlets of interfacial elasto-inertial microfluidic channel, (III) the CEA units, (IV) the outlets of symmetrical CEA flow channel. (C) Structure diagram of the integrated device made of three-layer polymer films and fixtures. (D and E) Photograph of the chip (D) and the assembled device (E).

of blood cells can be achieved, thereby improving the purity of the enriched tumor cells.

2.2 Device design and fabrication

The microchannel of our device was composed of an interfacial elasto-inertial microfluidic channel and a symmetric CEA channel in series, and the heights of the both channels were consistent and set to be 50 μm. The interfacial elasto-inertial microfluidic channel employed a wave-shaped design scheme to reduce the footprint of the channel and its total deployed length reached 38 mm. The symmetric CEA channel consisted of 60 square chambers with side lengths of 240 μm and these square chambers were connected by the rectangular channels with a length of 260 μm and a width of 50 μm. To balance the flow resistance of the series-connected symmetrical CEA channel, the waste liquid outlets on both sides of the interfacial elasto-inertial microfluidic channel were extended. Detailed dimensions on the microchannel design used in this work can be found in Fig. S1.† Low-cost and rapid fabrication of the chip was achieved using the laser cutting of polymer films. Our device consisted of fixtures and three layers of sequentially spliced polymer film layers (see Fig. 1C). The material of middle channel layer used the polysiloxane film with a thickness of 50 μm, while the cover and bottom layers were made of polyethylene terephthalate (PET) films. Briefly, the cover layer, middle channel layer, and bottom layer were cut into predetermined shapes by using a UV laser cutting system (15 W, 355 nm laser source, TH-UV200A, Tianhong) and then the three film layers were

sequentially cleaned and bonded by using an oxygen plasma (PDC-002, Harrick Plasma). The photograph of the fabricated chip was illustrated in Fig. 1D. The microchannels were made visible by injecting red ink. Finally, the chip was fixed and compressed by two polymethyl methacrylate (PMMA) cover and bottom fixtures and the introduction and output of the sample were accomplished by installing conduits on the cover fixture (see Fig. 1E). The dark red, blue, light red, and green arrows indicate the two sample fluid inlets, the sheath fluid inlet, the two waste fluid outlets, and the target collection fluid outlet, respectively.

2.3 Sample preparation

Cell suspensions were prepared by mixing bloods with three types of tumor cells, respectively. Sheath fluid was prepared by adding hyaluronic acid (HA, Shanghai Future Industrial) with a molecular weight of 1650 kDa to phosphate-buffered saline (PBS, Sigma-Aldrich) buffer at a concentration of 50 ppm. Blood samples collected from healthy consenting volunteers were diluted for 10 folds, 100 folds, and 1000 folds with PBS to determine the effect of cell concentration on device separation performance. Human breast cancer cells (MCF-7 and MDA-MB-231) and human lung cancer cells (A549) were used to mimic MTCs in clinical MPPE samples. MCF-7, MDA-MB-231, and A549 cells were cultured in medias (1640, L15, and F-12k, Thermo Fisher Scientific) containing 1% penicillin–streptomycin (Thermo Fisher Scientific) and 10% fetal bovine serum (Thermo Fisher Scientific) under the condition of 5% CO_2 and 37 °C, respectively. After

dissociating using 0.25% trypsin–EDTA solution (Thermo Fisher Scientific), MCF-7, MDA-MB-231, and A549 cells were re-suspended in PBS buffer to obtain tumor cell suspensions with concentrations of 10^4 and 10^3 counts per mL, respectively. To better observe the trajectory of tumor cells and distinguish the tumor cells from blood cells, the prepared tumor cells were fluorescently stained with calcein-AM solution (C481, Invitgen) at 37 °C and mixed with blood cells to simulate clinical MPPE samples.

Clinical MPPE samples were collected from cancer patients with advanced metastatic hemangiosarcoma, lung adenocarcinoma, lymphoma, liver cancer, and ovarian cancer. The collection and use of blood and MPPE samples were approved by the institutional committee of the Institutional Ethical Committee (IEC) for Clinical Research of Zhongda Hospital (Southeast University) under NO. 2020ZDSYLL043-Y01 and informed consent was obtained from the both volunteers and patients. All experiments were performed in compliance with the Chinese laws and following the institutional guidelines. After processing untreated clinical MPPE samples with our CEICS device, immunofluorescence staining was applied to the collected cells to identify target MTCs from WBCs. Briefly, all cells were adhered to the slide by incubating the collected sample on the adhesive slide for 30 minutes. Then, the cells were fixed by −20 °C methanol solution for 5 minutes and blocked with blocking solution (PBS buffer containing 3% goat serum (Thermo Fisher Scientific), 3% bovine serum albumin (BSA, Sigma-Aldrich), and 3% fetal bovine serum (FBS, Thermo Fisher Scientific)) for 30 minutes. Afterwards, the cells were incubated with Anti-Hu CD45 (Thermo Fisher Scientific) antibody containing fluorophore and Anti-Pan Cytokeratin (CK, Thermo Fisher Scientific) antibody containing fluorophore at 4 °C for 12 h. Before mounting with coverslips (Matsunami), cell nuclei were stained by adding antifade mounting medium with DAPI (Vector Laboratories). Therefore, target MTCs and WBCs were identified by CD45−/CK+/DAPI+ and CD45+/CK−/DAPI+, respectively.

2.4 Experimental setup and data analysis

The prepared samples and sheath fluid were injected at different flow rates using two syringe pumps (Legato270, KD Scientific). The CEICS device was fixed on the platform of an inverted fluorescence microscope (IX71, Olympus) and the movements of cells in the channel of the device were observed. Images of cell movements in fluorescence and bright modes were continuously captured using a high-speed camera (Phantom V611, Vision Research) and these discrete images were stacked by image processing software ImageJ (National Institutes of Health, USA) to illustrate the cell movement trajectories. To characterize the separation performance of the CEICS device, the concentrations of WBCs and stained tumor cells in the collected liquids after separation were measured using an automated cell counter (Countess II FL, Thermo Fisher Scientific). The recovery ratio

and purity of tumor cells were analyzed based on the collected liquids from three outlets. Recovery ratio was defined as the ratio of the number of tumor cells recovered from the target outlet to the number of tumor cells injected into the inlets, while purity was the proportion of tumor cells to the total cells recovered from the target outlet.

3. Results and discussion

3.1 Understanding the separation performances of single-stage channels

Due to the significant impact of experimental conditions (e.g., flow-rate ratio (FR), cell concentration, and throughput) on device separation performances, we first explored the separation performances of single-stage channels before testing our CEICS device. For the interfacial elasto-inertial microfluidic channel, we first tested the effect of the FR of sheath to sample fluids on the lateral migration of tumor cells. The 50 ppm HA solutions and pre-stained MCF-7 cell suspension with a concentration of 10^4 cells per mL were injected into the channel at FR values of 0.25, 0.5, 1, and 2, respectively. The total flow rate of the sheath and sample fluids was fixed at 240 μL min^{-1}. The fluorescence trajectories of MCF-7 cells at the channel outlet are shown in Fig. 2A. It was found that MCF-7 cells were collected from the middle outlet under all FR conditions. However, for FR = 0.25 and 0.5, the wide sample flows on both sides of channel seemed to be unfavorable for the cell interfacial separation, resulting in a band-like focusing of MCF-7 cells at the channel center. In addition, the low sheath flow rate could cause a part of the sample fluids from both sides to flow into the middle outlet, which deteriorated the separation performance. For FR > 1, although the efficient focusing of MCF-7 cells at the channel center were achieved, the further increase of FR reduced the actual processing throughput of samples. Therefore, FR was determined to be 1 for subsequent experiments. Cell concentrations in MPPEs from different cancer patients have a wide distribution range of 10^4–10^8 cells per mL. Therefore, in order to achieve pretreatment-free separation of MPPE samples (especially bloody MPPEs), it is necessary to ensure that our interfacial elasto-inertial microfluidic channel can efficiently remove a large number of background cells under high cell concentration conditions. We next analyzed the effect of cell concentration on interfacial elasto-inertial separation performance. The whole blood samples with different cell concentrations (10^6–10^8 cells per mL) were injected into the channel, respectively. The distributions of blood cells at the channel outlet under different cell concentrations are depicted in Fig. 2B. It was found that for samples with different cell concentrations, the blood cells were well retained in the sample flow and could be removed from the side outlets. Although a small part of blood cells were squeezed into the sheath flow due to the violent collisions between cells at a high cell concentration of 10^8 cells per mL, these escaped cells could be further removed in the next-stage symmetrical CEA channel. The
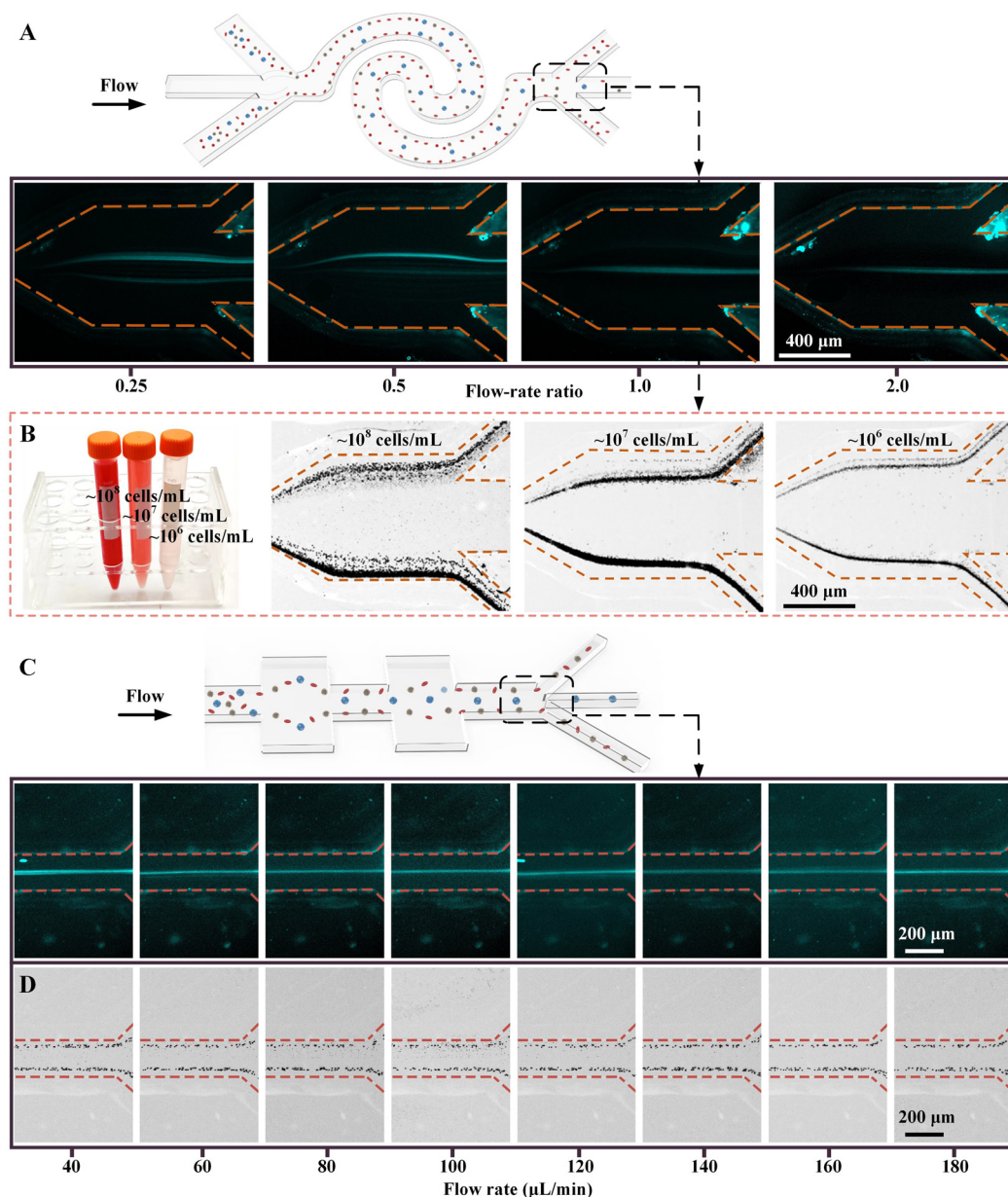
Fig. 2 (A) Fluorescence trajectories of MCF-7 cells at the outlets of interfacial elasto-inertial microfluidic channel. (B) Distributions of blood cells at the outlets of interfacial elasto-inertial microfluidic channel under different cell concentrations. (C) Fluorescence trajectories of MCF-7 cells at the outlets of symmetrical CEA channel. (D) Distribution of blood cells at the outlets of symmetrical CEA channel.

above results demonstrated the ability of our interfacial elasto-inertial microfluidic channel to directly remove blood cells from samples with different cell concentrations.

Due to the diversion of the waste liquid outlets on both sides of the interfacial elasto-inertial microfluidic channel, the throughput of samples entering the symmetrical CEA channel would be reduced. To ensure efficient removal of escaped blood cells while achieving the integration design of the CEICS device, we next investigated the optimal flow rate ranges of symmetrical CEA channel for cell separation. The cell concentration of MCF-7 cell suspension and blood cell suspension were set to $\sim 10^4$ cells per mL and $\sim 10^6$ cells per mL, respectively. The MCF-7 cell suspension and blood cell suspension were pumped into the

symmetric CEA channel at the flow rates ranging from 40 to 180 μL min^{-1}, respectively. The fluorescence trajectories of MCF-7 cells at the channel outlets are shown in Fig. 2C. MCF-7 cells were found to be focused at the channel center and could be enriched from the middle outlet during the whole flow-rate range. Meanwhile, the blood cells were focused at both sides of the channel and could be removed from the side outlets of the channel (see Fig. 2D). Therefore, the symmetric CEA channel can achieve efficient separation of tumor cells and blood cells over a wide range of flow rates. Based on the performance characterization results of the above two channels, we set the fluid throughput entering the symmetrical CEA channel to be 1/3 of the total throughput at the inlet.

3.2 Characterization of the separation performance of CEICS device

Next, blood samples spiked with different tumor cells were used to characterize the separation performances of the CEICS device. The cell concentration of blood samples was set to $\sim10^7$ cells per mL. The blood sample spiked with pre-stained MCF-7 cells at a concentration of $\sim10^4$ cells per mL and the 50 ppm HA solution were pumped into the CEICS device at the flow rate of 120 μL min^{-1}, respectively. The throughput of the device is $>10^6$ cells per min. Fig. 3A shows the bright and fluorescence trajectories of cells at the inlets, at the outlets of interfacial elasto-inertial microfluidic channel, and at the outlets of symmetric CEA channel. It was found that the tumor cells and blood cells mixed in the sample fluids were squeezed to both sides of the channel by the sheath fluid at inlet, and co-flowed along the channel (see i in Fig. 3A). With flowing along the interfacial elasto-inertial microfluidic channel, tumor cells gradually passed through the fluid interface into the sheath fluid and migrated towards the channel center, while blood cells were restricted by the fluid interface and remained in the sample flow. It was clearly observed from ii in Fig. 3A that the majority of the blood cells were removed successfully

through outlet 1. However, a small number of blood cells also passed through the fluid interface and entered the symmetric CEA channel together with tumor cells. Under the elasto-inertial effect of the symmetric CEA channel, the escaped blood cells were focused to both sides of the channel and removed from outlet 2, while the tumor cells still maintained a single-line focusing in the channel center (see iii in Fig. 3A). The bright and fluorescence microscopic images of the liquids collected from each outlet are depicted in Fig. 3B, which demonstrated that high-purity tumor cells were obtained at outlet 3 after separation. To further evaluate the separation performances of the CEICS device, the recovery ratio and purity of tumor cells were analyzed based on the collected liquids from three outlets. In addition, we separated the blood samples spiked with A549 and MDA-MB-231 cells using our CEICS device. The recovery ratios and purities of MCF-7, A549, and MDA-MB-231 cells are shown in Fig. 3C. After the cascaded elasto-inertial separation, the removal ratios of blood cells for the samples spiked with MCF-7, A549, and MDA-MB-231 cells were 99.93% ± 0.02%, 99.89% ± 0.02%, and 99.93% ± 0.03%, respectively. MCF-7, A549, and MDA-MB-231 cells achieved recovery ratios of 95.17% ± 2.30%, 97.17% ± 1.16%, and 94.87% ± 2.20%, respectively. The purities of MCF-7, A549, and
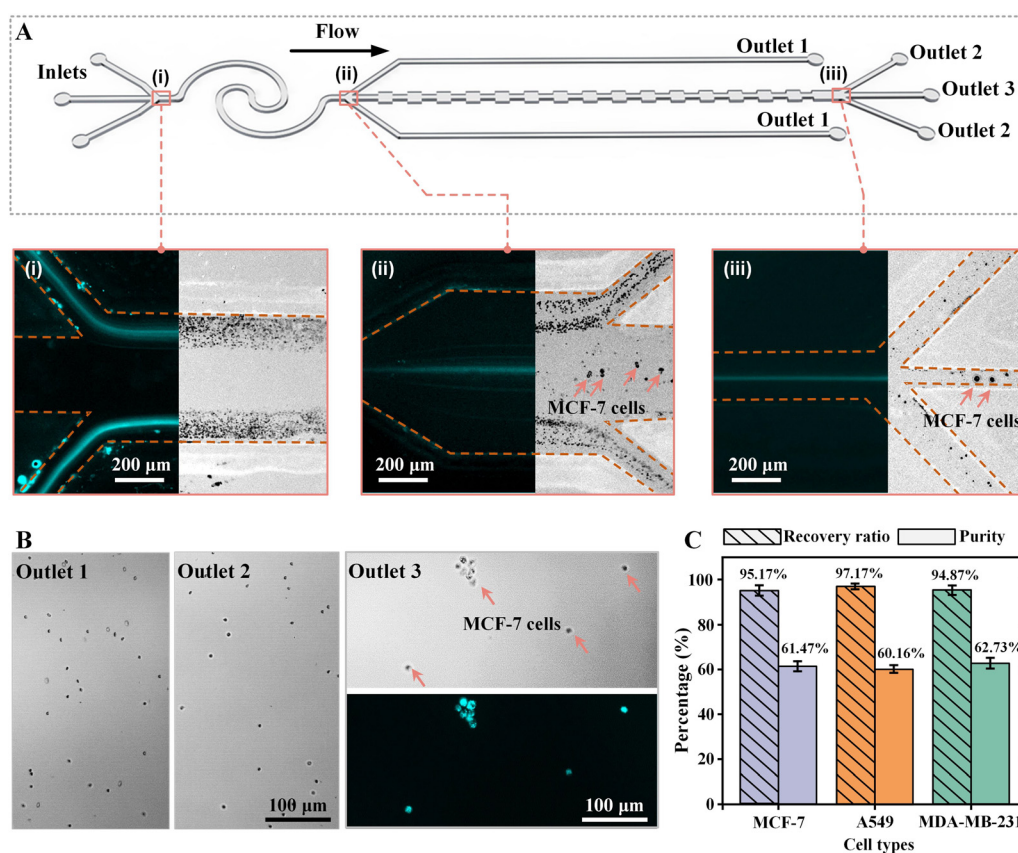

Fig. 3 Characterization of cell separation performance. (A) Bright and fluorescence images illustrating the cell distributions at the inlet (i), at the outlets of interfacial elasto-inertial microfluidic channel (ii), and at the outlets of symmetric CEA channel (iii). The tumor cells were stained before being spiked into the diluted blood samples. The fluorescent streams in the fluorescence images indicate the trajectories of the stained tumor cells. (B) Bright and fluorescence microscopic images of the liquids collected from the three outlets of the CEICS device after separation. (C) Separation performances of the CEICS device for separating different tumor cells with concentrations of $\sim10^4$ cells per mL from blood cells.

MDA-MB-231 cells were 61.47% ± 2.37%, 60.16% ± 1.74%, and 62.73% ± 2.46%, respectively. The aforementioned results demonstrate the excellent performance of the CEICS device for efficiently separating three tumor cells with an average recovery of ~95% and an average purity of ~61%, respectively. In addition, we explored the ability of our device to process blood samples spiked with lower concentrations of tumor cells. The concentration of tumor cells spiked into the blood sample was reduced to 10^3 cells per mL. The bright and fluorescence trajectories of cells at the three regions and microscopic images of the liquids collected from the three outlets are shown in Fig. S2 and S3.† It was found that well separation and enrichment of tumor cells could still be accomplished. Quantitative separation results showed that the purities of MCF-7, A549, and MDA-MB-231 cells decreased to 33.14% ± 4.59%, 33.31% ± 3.57%, and 34.85% ± 6.05%, respectively (see Fig. S4†). The reason for the purity decrease was due to the large reduction in the number of spiked tumor cells, while the removal rate of blood cells was not greatly affected. What is more, the change in tumor cell concentration did not affect the recovery efficiency of three tumor cells of our device.

3.3 Pretreatment-free, high-recovery-ratio, and high-purity separation of MTCs from clinical MPPEs

After separation performance characterization, we applied our device to the enrichment and purification of MTCs from clinical MPPEs. Untreated MPPE samples from five different

cancer patients (CP) and HA solution were sequentially pumped into CEICS device at a total flow rate of 240 μL min^{-1} (FR = 1). The detailed clinical information on the five patients can be found in Table S3.† Fig. 4A shows the cell distributions at the outlets of the interfacial elasto-inertial microfluidic channel and at the symmetrical CEA channel. It was found that the large-sized MTCs were focused at the center of the two channels and enriched from the middle outlets, while the blood cells were effectively removed under the cascaded elasto-inertial separation. Utilizing immunofluorescence staining, MTCs and WBCs in the collected liquids from outlet 3 were identified and counted. Fluorescence microscopic images of the separated MPPE samples after immunofluorescence staining are shown in Fig. 4B. The purified MTCs (CK+, CD45−, and DAPI+) and some residual WBCs (CK−, CD45+, and DAPI+) could be clearly observed in the sampling window. Based on the results of immunofluorescence staining, the numbers and purities of MTCs in the collected liquids of five MPPEs after cascaded elasto-inertial separation were determined. The numbers of MTCs detected in MPPE samples of hemangiosarcoma, lung adenocarcinoma, lymphoma, liver cancer, and ovarian cancer were 67, 45, 152, 270, and 88 cells per mL, respectively. In addition, the purities of MTCs from the five samples were 18.98%, 28.66%, 20.76%, 33.33%, and 21.36%, respectively. Compared with cancer cell line samples, the purity of the separated MTCs from clinical samples is reduced, which may be due to the high size heterogeneity of
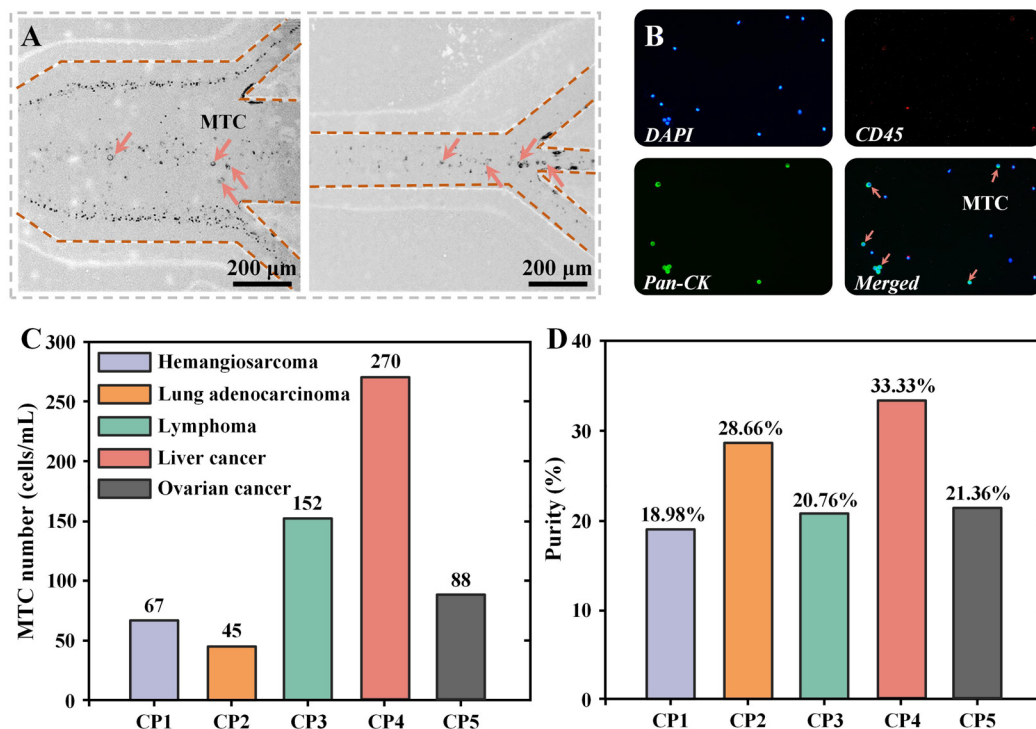

Fig. 4 Separation of MTCs from clinical pleural and peritoneal effusions. (A) Microscopy image illustrating the cell distributions at the outlets of interfacial elasto-inertial microfluidic channel and symmetrical CEA channel. (B) Fluorescence microscopic images of the separated MPPE samples after immunofluorescence staining. (C and D) Recovered numbers (C) and purities (D) of MTCs from the MPPE samples of five patients with different cancers.

cells in clinical samples. These results proved that our CEICS device could realize the pretreatment-free, high-recovery-ratio, and high-purity separation of MTCs from clinical MPPEs. Benefiting from the label-free operation, the purified tumor cells still maintain a good activity and can be used for subsequent applications, such as single-cell sequencing, *in vitro* culture, and drug resistance testing. We envision that our device can be used for the efficient separation of tumor cells from various blood, body fluids, and effusions, providing new insights into cytological examination.

4. Conclusions

In this work, a CEICS device was developed by integrating an interfacial elasto-inertial microfluidic channel with a symmetric CEA channel for pretreatment-free, high-recovery-ratio, and high-purity separation of MTCs from clinical MPPEs. The effects of experimental parameters (*i.e.*, flow-rate ratio, cell concentration, and cell size) on separation performance in two single-stage channels were first systematically characterized. Then, the performances of the integrated CEICS device were characterized under optimized parameters. The experimental results of three tumor cells (MCF-7, MDA-MB-231, and A549 cells) demonstrated the excellent performance of the CEICS device with an average recovery of ~95% and an average purity of ~61%, respectively. Finally, the enrichment and purification of MTCs in clinical MPPEs from patients with different cancers were successfully achieved using our CEICS device. The designed CEICS device may provide a preparation tool for improving the sensitivity and efficiency of cytological examination of MPPE samples.

Conflicts of interest

There are no conflicts to declare.

Acknowledgements

References

1 Q. Ma, X. He, B. Zhang, F. Guo, X. Ou, Q. Yang, P. Shu, Y. Chen, K. Li and G. Gao, *et al.* A PD-L1-targeting chimeric switch receptor enhances efficacy of CAR-T cell for pleural and peritoneal metastasis, *Signal Transduction Targeted Ther.*, 2022, **7**(1), 380.

2 Y. Sun, Y. Hu, C. Wan, J. F. Lovell, H. Jin and K. Yang, Local biomaterial-assisted antitumour immunotherapy for effusions in the pleural and peritoneal cavities caused by malignancies, *Biomater. Sci.*, 2021, **9**(19), 6381–6390.

3 G. Baburaj, R. R. Damerla, K. S. Udupa, P. Parida, M. Munisamy, J. Kolesar and M. Rao, Liquid biopsy approaches for pleural effusion in lung cancer patients, *Mol. Biol. Rep.*, 2020, **47**(10), 8179–8187.

4 N. R. Desai and H. J. Lee, Diagnosis and management of malignant pleural effusions: state of the art in 2017, *J. Thorac. Dis.*, 2017, **9**, S1111–S1122.

5 J. M. Thomas and A. I. Musani, Malignant Pleural Effusions A Review, *Clin. Chest Med*, 2013, **34**(3), 459–471.

6 C.-G. Wu, F. Chiovaro, A. Curioni, R. Casanova and A. Soltermann, In vitro cell culture of patient derived malignant pleural and peritoneal effusions for personalised drug screening, *J. Transl. Med.*, 2020, **18**(1), 163.

7 J. M. Porcel, Diagnosis and characterization of malignant effusions through pleural fluid cytological examination, *Curr. Opin. Pulm. Med.*, 2019, **25**(4), 362–368.

8 V. Pillai, E. S. Cibas and D. M. Dorfman, A Simplified Flow Cytometric Immunophenotyping Procedure for the Diagnosis of Effusions Caused by Epithelial Malignancies, *Am. J. Clin. Pathol.*, 2013, **139**(5), 672–681.

9 H. Motherby, B. Nadjari, P. Friegel, J. Kohaus, U. Ramp and A. Bocking, Diagnostic accuracy of effusion cytology, *Diagn. Cytopathol.*, 1999, **20**(6), 350–357.

10 N. Xiang and Z. Ni, Inertial microfluidics: current status, challenges, and future opportunities, *Lab Chip*, 2022, **22**(24), 4792–4804.

11 N. Lu, H. M. Tay, C. Petchakup, L. He, L. Gong, K. K. Maw, S. Y. Leong, W. W. Lok, H. B. Ong and R. Guo, *et al.* Label-free microfluidic cell sorting and detection for rapid blood analysis, *Lab Chip*, 2023, **23**(5), 1226–1257.

12 C. Macaraniag, Q. Luan, J. Zhou and I. Papautsky, Microfluidic techniques for isolation, formation, and characterization of circulating tumor cells and clusters, *APL Bioeng.*, 2022, **6**(3), 031501.

13 X. Xu, X. Huang, J. Sun, R. Wang, J. Yao, W. Han, M. Wei, J. Chen, J. Guo and L. Sun, *et al.* Recent progress of inertial microfluidic-based cell separation, *Analyst*, 2021, **146**(23), 7070–7086.

14 X. Lu, C. Liu, G. Hu and X. Xuan, Particle manipulations in non-Newtonian microfluidics: A review, *J. Colloid Interface Sci.*, 2017, **500**, 182–201.

15 L. M. Lee, G. J. J. Klarmann, D. W. W. Haithcock, Y. Wang, K. H. H. Bhatt, B. Prabhakarpandian, K. Pant, L. M. M. Alvarez and E. Lai, Label-free enrichment of human adipose-derived stem cells using a continuous microfluidic sorting cascade, *Lab Chip*, 2023, **23**(8), 2131–2140.

16 S. Razavi Bazaz, A. Mihandust, R. Salomon, H. A. N. Joushani, W. Li, H. A. Amiri, F. Mirakhorli, S. Zhand, J. Shrestha and M. Miansari, *et al.* Zigzag microchannel for rigid inertial separation and enrichment(Z-RISE) of cells and particles, *Lab Chip*, 2022, **22**(21), 4093–4109.

17 H. Cha, H. Fallahi, Y. Dai, S. Yadav, S. Hettiarachchi, A. McNamee, H. An, N. Xiang, N.-T. Nguyen and J. Zhang, Tuning particle inertial separation in sinusoidal channels by embedding periodic obstacle microstructures, *Lab Chip*, 2022, **22**(15), 2789–2800.

18 M. Boya, T. Ozkaya-Ahmadov, B. E. Swain, C.-H. Chu, N. Asmare, O. Civelekoglu, R. Liu, D. Lee, S. Tobia and S. Biliya, *et al.* High throughput, label-free isolation of circulating tumor cell clusters in meshed microwells, *Nat. Commun.*, 2022, **13**(1), 3385.

19 K. J. Smith, J. A. Jana, A. Kaehr, E. Purcell, T. Opdycke, C. Paoletti, L. Cooling, D. H. Thamm, D. F. Hayes and S. Nagrath, Inertial focusing of circulating tumor cells in whole blood at high flow rates using the microfluidic CTCKey(TM) device for CTC enrichment, *Lab Chip*, 2021, **21**(18), 3559–3572.

20 K. Shirai, G. Guan, M. Tan, X. Peng, Y. Oka, Y. Takahashi, A. A. S. Bhagat, M. Yanagida, S. Iwanaga and N. Matsubara, *et al.* Hybrid double-spiral microfluidic chip for RBC-lysis-free enrichment of rare cells from whole blood, *Lab Chip*, 2022, **22**(22), 4418–4429.

21 N. Xiang and Z. Ni, High-throughput concentration of rare malignant tumor cells from large-volume effusions by multistage inertial microfluidics, *Lab Chip*, 2022, **22**(4), 757–767.

22 F. Jiang and N. Xiang, Integrated Microfluidic Handheld Cell Sorter for High-Throughput Label-Free Malignant Tumor Cell Sorting, *Anal. Chem.*, 2022, **94**(3), 1859–1866.

23 C. Ni, Z. Zhu, Z. Zhou and N. Xiang, High-Throughput Separation and Enrichment of Rare Malignant Tumor Cells from Large-Volume Effusions by Inertial Microfluidics, *Methods in molecular biology*, Clifton, N.J., 2023, vol. 2679, pp. 193–206.

24 Z. Zhu, D. Wu, S. Li, Y. Han, N. Xiang, C. Wang and Z. Ni, A polymer-film inertial microfluidic sorter fabricated by jigsaw puzzle method for precise size-based cell separation, *Anal. Chim. Acta*, 2021, **1143**, 306–314.

25 M. R. Condina, B. A. Dilmetz, S. R. Bazaz, J. Meneses, M. E. Warkiani and P. Hoffmann, Rapid separation and identification of beer spoilage bacteria by inertial microfluidics and MALDI-TOF mass spectrometry, *Lab Chip*, 2019, **19**(11), 1961–1970.

26 A. S. Rzhevskiy, A. Y. Kapitannikova, S. A. Vasilescu, T. A. Karashaeva, S. R. Bazaz, M. S. Taratkin, D. V. Enikeev, V. Y. Lekarev, E. V. Shpot and D. V. Butnaru, *et al.* Isolation of Circulating Tumor Cells from Seminal Fluid of Patients with Prostate Cancer Using Inertial Microfluidics, *Cancers*, 2022, **14**(14), 3364.

27 J. Shrestha, S. R. Bazaz, L. Ding, S. Vasilescu, S. Idrees, B. Soderstrom, P. M. Hansbro, M. Ghadiri and M. E. Warkiani, Rapid separation of bacteria from primary nasal samples using inertial microfluidics, *Lab Chip*, 2022, **23**(1), 146–156.

28 D. Yuan, S. Yan, J. Zhang, R. M. Guijt, Q. Zhao and W. Li, Sheathless Separation of Cyanobacterial Anabaena by Shape Using Viscoelastic Microfluidics, *Anal. Chem.*, 2021, **93**(37), 12648–12654.

29 X. Lu, J. J. M. Chow, S. H. Koo, B. Jiang, T. Y. Tan, D. Yang and Y. Ai, Sheathless and high-throughput elasto-inertial bacterial sorting for enhancing molecular diagnosis of bloodstream infection, *Lab Chip*, 2021, **21**(11), 2163–2177.

30 R. J. Gillams, V. Calero, R. Fernandez-Mateo and H. Morgan, Electrokinetic deterministic lateral displacement for fractionation of vesicles and nano-particles, *Lab Chip*, 2022, **22**(20), 3869–3876.

31 V. Varmazyari, H. Ghafoorifard, H. Habibiyan, M. Ebrahimi and S. Ghafouri-Fard, A microfluidic device for label-free separation sensitivity enhancement of circulating tumor cells of various and similar size, *J. Mol. Liq.*, 2022, **349**, 118192.

32 H. Udono, Numerical investigations of strong hydrodynamic interaction between neighboring particles inertially driven in microfluidic flows, *Adv. Powder Technol.*, 2020, **31**(9), 4107–4118.

33 S. S. Kuntaegowdanahalli, A. A. S. Bhagat, G. Kumar and I. Papautsky, Inertial microfluidics for continuous particle separation in spiral microchannels, *Lab Chip*, 2009, **9**(20), 2973–2980.

34 H. Ren, Z. Zhu, N. Xiang, H. Wang, T. Zheng, H. An, N. Nam-Trung and J. Zhang, Multiplexed serpentine microchannels for high-throughput sorting of disseminated tumor cells from malignant pleural effusion, *Sens. Actuators, B*, 2021, **337**, 129758.

35 C. Wang, Y. Chen, X. Gu, X. Zhang, C. Gao, L. Dong, S. Zheng, S. Feng and N. Xiang, Low-cost polymer-film spiral inertial microfluidic device for label-free separation of malignant tumor cells, *Electrophoresis*, 2022, **43**(3), 464–471.

36 Z. Zhu, S. Li, D. Wu, H. Ren, C. Ni, C. Wang, N. Xiang and Z. Ni, High-throughput and label-free enrichment of malignant tumor cells and clusters from pleural and peritoneal effusions using inertial microfluidics, *Lab Chip*, 2022, **22**(11), 2097–2106.

37 S. Yang, J. Y. Kim, S. J. Lee, S. S. Lee and J. M. Kim, Sheathless elasto-inertial particle focusing and continuous separation in a straight rectangular microchannel, *Lab Chip*, 2011, **11**(2), 266–273.

38 T. Zhang, A. K. Cain, L. Semenec, J. V. Pereira, Y. Hosokawa, Y. Yalikun and M. Li, Bacteria separation and enrichment using viscoelastic flows in a straight microchannel, *Sens. Actuators, B*, 2023, **390**, 133918.

39 F. Tian, W. Zhang, L. Cai, S. Li, G. Hu, Y. Cong, C. Liu, T. Li and J. Sun, Microfluidic co-flow of Newtonian and viscoelastic fluids for high-resolution separation of microparticles, *Lab Chip*, 2017, **17**(18), 3078–3085.

40 F. Tian, L. Cai, J. Chang, S. Li, C. Liu, T. Li and J. Sun, Label-free isolation of rare tumor cells from untreated whole blood by interfacial viscoelastic microfluidics, *Lab Chip*, 2018, **18**(22), 3436–3445.

41 M. A. Faridi, H. Ramachandraiah, I. Banerjee, S. Ardabili, S. Zelenin and A. Russom, Elasto-inertial microfluidics for bacteria separation from whole blood for sepsis diagnostics, *J. Nanobiotechnol.*, 2017, **15**, 1–9.

42 D. Yuan, S. H. Tan, R. Sluyter, Q. Zhao, S. Yan, N. T. Nguyen, J. Guo, J. Zhang and W. Li, On-Chip Microparticle and Cell Washing Using Coflow of Viscoelastic Fluid and Newtonian Fluid, *Anal. Chem.*, 2017, **89**(17), 9574–9582.

43 X. Shi, L. Liu, W. Cao, G. Zhu and W. Tan, A Dean-flow-coupled interfacial viscoelastic fluid for microparticle separation applied in a cell smear method, *Analyst*, 2019, **144**(20), 5934–5946.

44 X. Shi, W. Tan, L. Liu, W. Cao, Y. Wang and G. Zhu, Separation of exfoliated tumor cells from viscoelastic pleural effusion using a microfluidic sandwich structure, *Anal. Bioanal. Chem.*, 2020, **412**(22), 5513–5523.

45 Y. Cheng, S. Zhang, L. Qin, J. Zhao, H. Song, Y. Yuan, J. Sun, F. Tian and C. Liu, Poly(ethylene oxide) Concentration Gradient-Based Microfluidic Isolation of Circulating Tumor Cells, *Anal. Chem.*, 2023, **95**, 3468–3475.

46 T. Zhang, A. K. Cain, L. Semenec, L. Liu, Y. Hosokawa, D. W. Inglis, Y. Yalikun and M. Li, Microfluidic Separation and Enrichment of Escherichia coli by Size Using Viscoelastic Flows, *Anal. Chem.*, 2023, **95**, 2561–2569.

47 N. Xiang, Z. Ni and D. Wu, High-throughput and high-purity separation of malignant tumor cells in pleural and peritoneal effusions using interfacial elasto-inertial microfluidics, *Sens. Diagn.*, 2023, **2**(4), 929–937.